Growth mechanism and optoelectronic properties of nanocrystalline In$_2$O$_3$ films prepared by chemical spray pyrolysis of metal-organic precursor

A. Moses Ezhil Raj[a], K.C. Lalithambika[b], V.S. Vidhya[c], G. Rajagopal[c], A. Thayumanavan[d], M. Jayachandran[c], C. Sanjeeviraja[e,*]

[a]*Department of Physics, Scott Christian College, Nagercoil 629003, India*
[b]*Department of Physics, SASTRA University, Thirumalai Samudram, Thanjavur 613402, India*
[c]*Central Electrochemical Research Institute, Karaikudi 630006, India*
[d]*AVVM Sri Pushpam College, Poondi 613503, India*
[e]*Department of Physics, Alagappa University, Karaikudi 630003, India*

Abstract

Thin films of indium oxide, In$_2$O$_3$, were deposited by chemical spray pyrolysis technique, using aqueous alcoholic solutions of indium acetylacetonate (In-acac) precursor, on glass substrates kept at temperatures between 300 and 500 °C. The structural, optical, and electrical properties have been investigated as a function of deposition temperature, precursor concentration, carrier gas pressure, and substrate-to-nozzle distance. X-ray diffraction studies showed that the formation of nanocrystalline In$_2$O$_3$ films is preferentially oriented along (2 2 2) plane. The surface morphological modifications with substrate temperature were observed using scanning electron and atomic force microscopic studies. Optical transmittance behavior of the films in the visible and IR region was strongly affected by the deposition parameters. The optical band gap values observed are between 3.53 and 3.68 eV. The long wavelength limit of refractive index is 1.83. The Hall mobility is found to vary from 23 to 37 cm^2/V s and carrier density is found nearly constant at about 10^{20} cm^{-3}.
© 2007 Elsevier B.V. All rights reserved.

1. Introduction

High optical transparency in the visible region more than 80%, low electrical resistivity less than 10^{-3} Ω cm and high infrared reflectivity make indium oxide (In$_2$O$_3$) a choice for many potential applications in the upcoming nanoelectronic building blocks. In$_2$O$_3$ is an n-type semiconductor with a wide band gap of about 3.6 eV that exhibits many size- and shape-dependent properties, based on which many new applications have been also explored. Indium oxide has C-type rare earth oxide structure with the space group of T_h^7(Ia3) that crystallites in the ordered vacancy structure with eight formula units. Among the 16 In atoms,

1/4 of the In atoms (In1) occupy the centers of the trigonally distorted octahedra (Wyckoff 8b position) and 3/4 of In atoms (In2) occupy the centers of tetragonally distorted octahedra (Wycoff 24d position) that ensure a good packing ratio [1]. In addition, In$_2$O$_3$ has single free electron-like band of s-character forming the bottom of the conduction band hybridized with highly dispersed O 2s states. The valence band edge arises from the O 2p states hybridized with In$_2$ 5d. This intriguing band structure results in uniform distribution of the charge that reduces the scattering to a minimum. Moreover, the high electrical conductivity due to mobility enhancement and Burstein–Moss shift can also be explained on the basis of dispersion of these bands. These interesting optical and electrical properties tailored to occur due to the modified structural packing and band structure makes this

*Corresponding author. Tel.: +91 4565 230251; fax: +91 4565 225202.
E-mail address:* sanjeeviraja@rediffmail.com (C. Sanjeeviraja).

material suitable for many novel optoelectronic device fabrications.

Among the transparent conducting oxide (TCO) materials, In_2O_3 is physically stable and chemically inert. As a transparent conductor, it exhibits characteristics similar to SnO_2 and is superior for applications in many aspects. Indium oxide can be used as a TCO material in optoelectronic devices, including thin film solar cells [2], gas sensors [3], electroluminescent devices and antireflection coatings [4], liquid crystal displays [5], electrochromic devices [6], photothermal devices [7], and light-emitting diodes [8]. Because In_2O_3 is mostly used in the form of films, it is generally characterized in terms of thin film properties, which are markedly different from the properties of bulk material. In addition, the properties of indium oxide thin films are dependent on the preparation conditions and related parameters. Several methods have been used to deposit these films like reactive evaporation [9], magnetron sputtering [10], pulsed laser deposition [11], electron beam evaporation [12], chemical vapor deposition (CVD) [13], sol–gel [14], and chemical spray pyrolysis [15]. Amongst these, chemical spray pyrolysis is cost-effective capable of producing large-area films and easy doping.

Transparent conducting films of indium oxide were prepared usually by spraying an alcoholic solution of $InCl_3$ [15–19] and sometimes using $InNO_3$. The solvents used are mainly ethanol/methanol mixed with water and rarely butyl acetate [16]. In the present study, a metal-organic salt of indium, indium acetylacetonate (In-acac), has been used as the precursor salt which was dissolved in 50 ml ethanol–water mixtures stabilized with 2 ml of hydrochloric acid.

The process parameters of chemical spray pyrolysis technique have profound influence on the film properties. Hence, a systematic optimization of each parameter has been carried out to deposit device-quality In_2O_3 films possessing high electrical conductivity and optical transmittance. The structural, optical, and electrical properties were investigated in detail and presented.

2. Experimental

The spray pyrolysis growth of In_2O_3 thin films was carried out in an indigenously made reaction chamber. The deposition setup consists of four sections, which include: (a) the precursor and carrier gas assembly connected to the spray nozzle, (b) the reaction chamber in which the substrate is heated, (c) the pumping and exhausting gas scrubbing systems, and (d) temperature controller/monitor assembly to control the substrate temperature. Fine droplets were sprayed onto the heated glass substrates (corning-7059) using an atomizer, which is made of glass having diameter of 0.5 mm. The precursor solution was prepared by dissolving In-acac in high-purity ethanol and deionized water in different proportions to make spray precursor solution of different concentrations (0.002–0.02 M). The solution was sprayed onto pre-cleaned glass

substrates held at temperature between 300 and 500 °C in steps of 50 °C. The substrate-to-nozzle distance (SND) was changed between 25 and 40 cm, and the carrier gas flow rate was varied from 0.2 to 0.5 kg/cm^2.

After deposition, the peel-off test was conducted to confirm the adhesivity of the In_2O_3 films on glass substrates, which showed well-adherent In_2O_3 films formed in the present study. The thicknesses of the films were then measured using Stylus profiler (Mitutoyo SJ-301). The thicknesses of the films were in the range 0.4–0.6 μm depending on the deposition conditions. X-ray diffraction (XRD; X'pert Pro) was used to analyze the crystal structure of the In_2O_3 films. Scanning electron microscopy (JEOL JSM-35 CF) and atomic force microscopy (Nanoscope-E AFM/STM) were used to evaluate the surface morphology of the films. Composition of the films was determined by Rutherford backscattering spectrometry (RBS) using 2 MeV He$^+$ ion beam. The optical transmittance studies were performed using the double-beam UV–vis–NIR spectrophotometer (Hitachi-3400) in the wavelength range of 300–1000 nm. The sheet resistance (R_{sh}) and resistivity (ρ) were measured using the four-point probe technique. The carrier density and mobility of carrier electron were estimated from the Hall effect measurement setup.

3. Result and discussions

3.1. Growth mechanism of In_2O_3 films

Indium oxide films were prepared with different In-acac concentrations of 0.002, 0.004, 0.008, 0.012, and 0.020 M at a substrate temperature of 400 °C. The precursor flow rate was maintained at 5 ml/min and SND was kept at 30 cm. The variation of film growth rate with the molar concentration of the precursor solution for two different ethanol–water solvent proportions (90:10 and 50:50) is shown in Fig. 1a and b, respectively.

It is evident that two types of growth mechanisms are involved during film formation. The growth rate is almost linear up to the concentration of 0.008 M beyond which a saturation in growth rate is observed for molarities greater than 0.008 M. The linear growth at low concentrations may be due to the continuous adsorption of the solution followed by the reaction between the adsorbed indium species and the solvent molecules. However, for higher molarity solutions, the available oxygen molecules of the solvent may not be sufficient to increase the growth rate and so the reactants on the surface of the substrate are saturated, which leads to the saturation of In_2O_3 layer growth. Also from Fig. 1a and b, it is inferred that the reevaporation of the 90:10 ethanol–water precursor is stronger with lower growth rate compared to that of 50:50 precursor with larger growth rate. Therefore, the films prepared from the 50:50 ethanol–water precursors were thicker, but the film surface was covered with white foggy patches with less transparency and impaired smoothness.
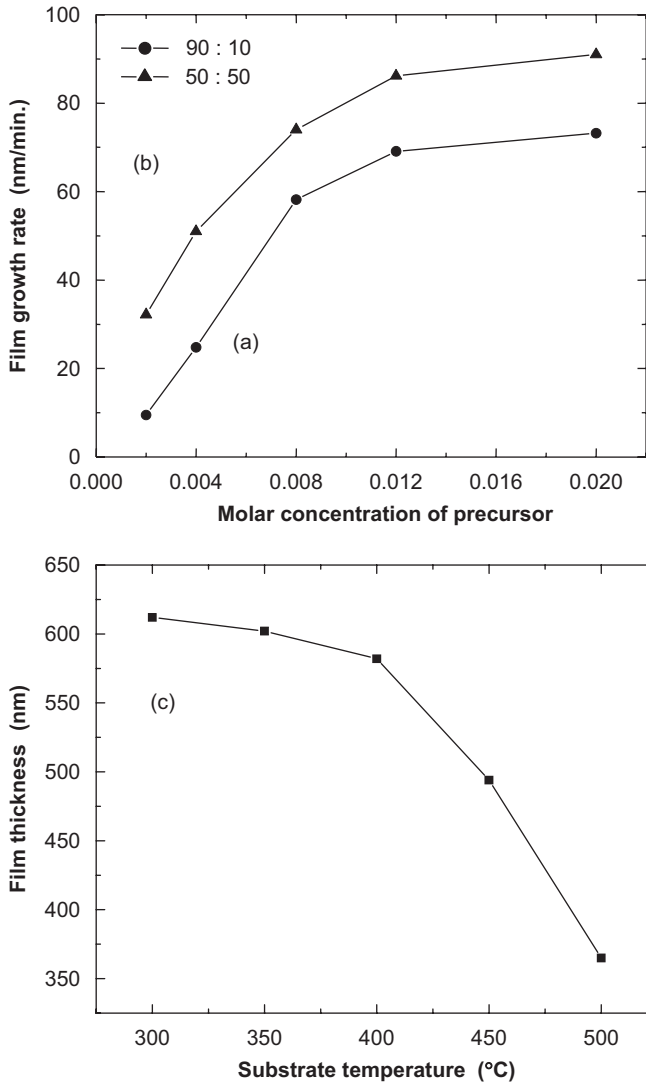
Fig. 1. Growth rate variation with molar concentration for ethanol–water ratio of (a) 90:10 and (b) 50:50. (c) Variation of film thickness with substrate temperature.

But, 90:10 ethanol–water precursor produced uniform films due to heterogeneous reactions. Based on these observations, it was fixed that a concentration of 0.008 M in 90:10 ethanol–water solvent was the suitable precursor solution for In_2O_3 thin film preparation.

Thickness variation of In_2O_3 films deposited at different substrate temperatures is shown in Fig. 1c. A constant volume (50 ml) of the precursor solution was sprayed at the rate of 5 ml/min. The film thickness was found decreasing with the increase of substrate temperature. This may be due to the reduction of precursor mass transfer to the substrate. The reduced mass transport is due to gas convection from the chamber, pushing the droplets away, which induces formation of crystallites in the vapor itself. This type of observations is reported for many oxide films prepared by the chemical spray pyrolysis technique [20]. Films deposited at 300 °C are thicker but the films were foggy in nature. At 400 °C, the fogginess completely disappeared and the

films were highly transparent. At higher temperatures (>400 °C), the film surface became powdery because of homogeneous nucleation and reaction.

3.2. Influence of process parameters on the In_2O_3 films

In order to study the influence of substrate temperature on composition and crystalline properties of In_2O_3 films, the precursor solution was sprayed onto heated glass substrates maintained at constant temperature between 300 and 500 °C. In all depositions, 50 ml of the solution was sprayed at a rate of 5 ml/min. Compressed air at a pressure of 0.4 kg/cm^2 was used and SND was 30 cm.

Structural developments of In_2O_3 thin films as a function of deposition temperature are shown in Fig. 2. The indium oxide films deposited between 350 and 500 °C are polycrystalline and showed (2 2 2) preferred orientation but with varied intensities. Amorphous nature is observed with a small peak at 30.42° for the films deposited at 300 °C and the increase of temperature leads to an improvement in crystallinity. The film prepared at 400 °C exhibits intense peaks at 30.56°, 35.45°, 51.03°, and 60.61° corresponding to the (2 2 2), (4 0 0), (4 4 0), and (6 2 2) planes, respectively, with specific orientation along (2 2 2) direction. These
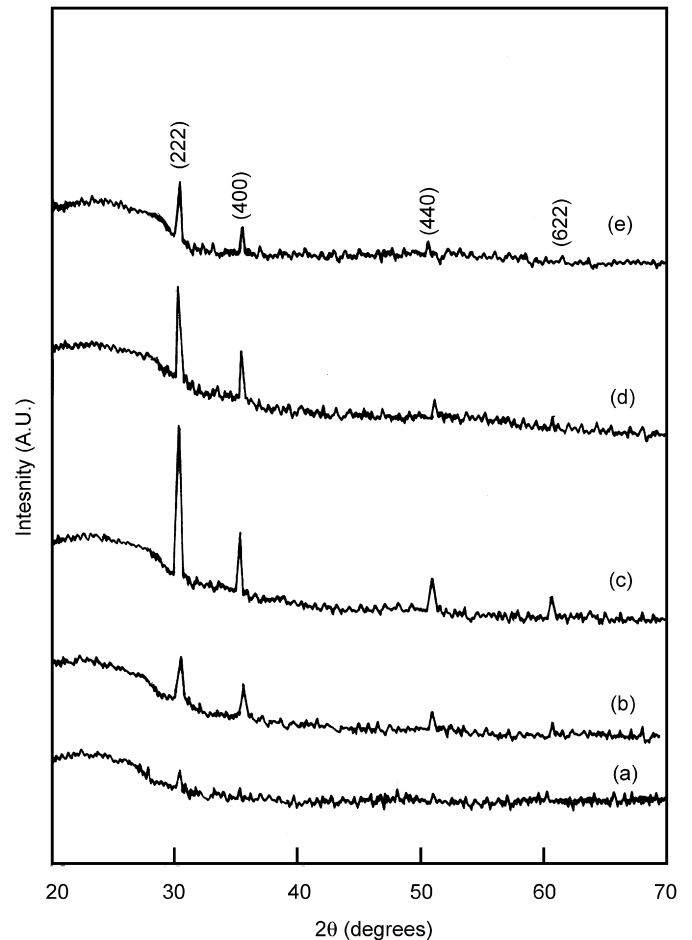

Fig. 2. XRD spectra of In_2O_3 films deposited at substrate temperatures: (a) 300 °C, (b) 350 °C, (c) 400 °C, (d) 450 °C, and (e) 500 °C.

Table 1
Measured grain size, dislocation density, and microstrain of In$_2$O$_3$ films deposited at different substrate temperatures

Substrate temperature (°C)	(2 2 2) interplanar distance, d (Å)	Lattice constant, a (Å)	Grain size, D (nm)	Microstrain, ε ($\times 10^{-3}$)	Dislocation density, δ ($\times 10^{14}$ lines cm^{-2})
300	2.934	10.164	22.1	1.63	10.88
350	2.932	10.157	27.7	1.30	6.93
400	2.930	10.150	35.8	1.01	4.17
450	2.934	10.164	40.9	0.88	3.17
500	2.933	10.160	43.0	0.084	0.28

peaks correspond to the body centered cubic (bcc) structure of In$_2$O$_3$ films indexed according to the JCPDS standards (Card No. 06-0416). At high-temperature depositions, the peak intensity decreases and this may be due to the evaporation of indium salt that leads to homogeneous nucleation, forming films with powdery surface and also with distorted crystal lattice [21].

The interplanar distance for (2 2 2) plane of the In$_2$O$_3$ films is found to be higher than the standard value of $d = 2.921$ Å. This indicates expansion of unit cell volume which in turn reveals the presence of stress in all the films. The microstructural properties and lattice disorders are studied from the analysis of XRD peaks. Due to the presence of stress, there must be strain and the associated lattice defects can be calculated by measuring the full-width at half-maximum (FWHM) values of the XRD peak and are listed in Table 1 for the preferentially oriented (2 2 2) plane of each film deposited at different temperatures. It is clear that the lattice constant values of all the In$_2$O$_3$ films are exceeding the bulk value $a = 10.11$ Å. However, the film deposited at 400 °C shows a minimum value of 10.15 Å among the others. In addition, it is evident that grain size of In$_2$O$_3$ films increases with increasing substrate temperature for the (2 2 2) oriented crystallites which is in accordance with the reported results for the doped In$_2$O$_3$ films [22].

The crystals defect parameters like microstrain and dislocation density show a decreasing trend with increase in substrate temperature. This type of change in strain may be due to the recrystallization process in the polycrystalline films. At high-temperature deposition, both the microstrain and dislocation density are minimum, which reveals the reduction in the concentration of lattice imperfections leading to preferred orientations [23].

Fig. 3 shows the XRD spectra of indium oxide films prepared at various molar concentrations (0.002–0.020 M) of In-acac in 50 ml of the solvent by keeping the other process parameters constant as mentioned earlier. As seen from the XRD spectra, all films are polycrystalline in nature with a cubic structure.

For the low molar precursor concentration (0.002 M), the deposited films are very thin and have lot of irregularities and exhibit amorphous nature. For further increase in molarity, the films show improved crystalline structure and the intensity of (2 2 2) plane increases to a
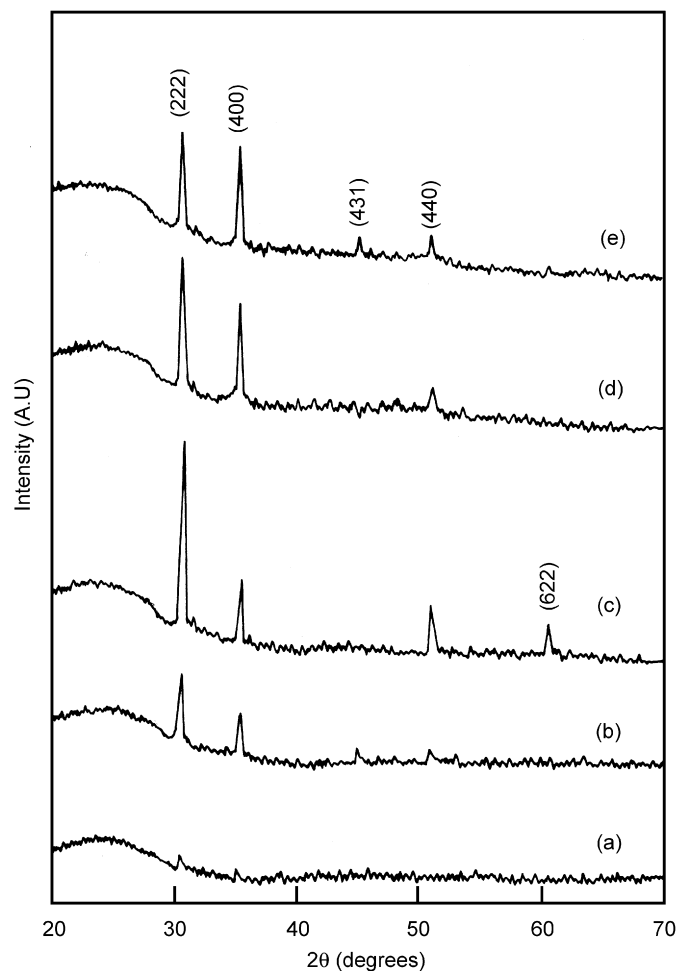

Fig. 3. Diffractograms of In$_2$O$_3$ films deposited from various molar concentrations of precursor solution: (a) 0.002 M, (b) 0.004 M, (c) 0.008 M, (d) 0.012 M, and (e) 0.02 M.

maximum up to a molarity of 0.008 M. Other planes (4 0 0), (4 4 0), and (6 2 2) are also present, but their intensities are lesser than the intensity of (2 2 2) plane. Above this precursor concentration, the intensity of (2 2 2) peak is reduced and that of (4 0 0) peak is slightly increased but is always less than the (2 2 2) peak. A similar change of growth pattern has also been observed for ZnO and SnO$_2$ [24] films. But, the films prepared with highly concentrated solution are electrically resistive and optically less transparent due to their structural disorder.
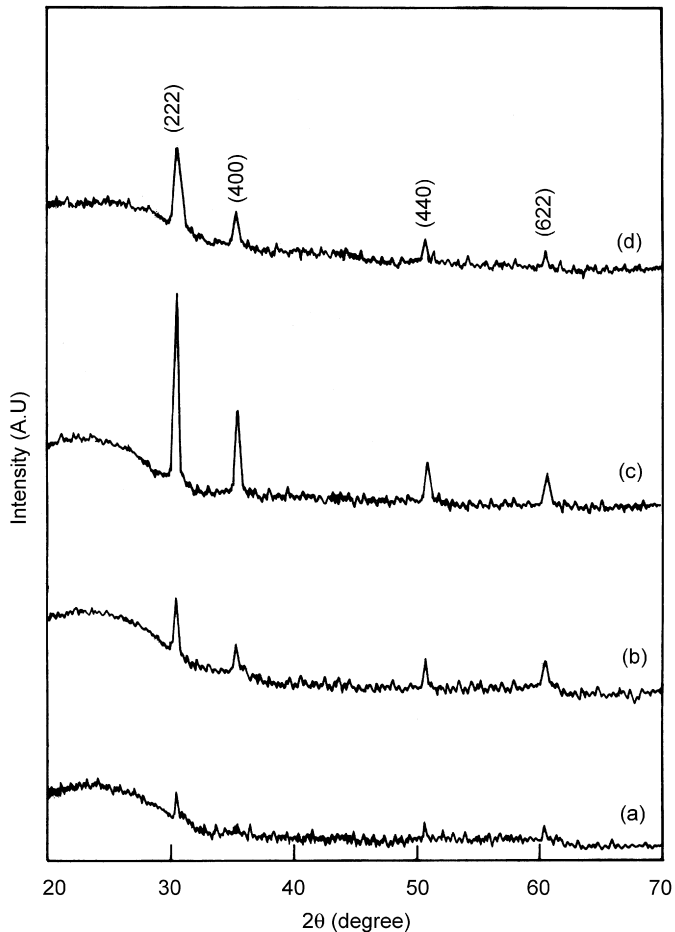
Fig. 4. XRD spectra of In_2O_3 films prepared at various carrier gas pressures: (a) $0.2\,kg/cm^2$, (b) $0.3\,kg/cm^2$, (c) $0.4\,kg/cm^2$, and (d) $0.5\,kg/cm^2$.

Table 2
Process parameters varied and optimized for In_2O_3 thin film preparation

Deposition parameters	Values
Precursor solute	Indium acetylacetonate
Precursor solvent	Ethanol + water (90:10)
Precursor concentration	0.002–0.02 M (0.008 M)
Precursor volume	50 ml
Precursor flow rate	5 ml/min
Carrier gas pressure	0.2–0.5 kg/cm² (0.4 kg/cm²)
Substrate–nozzle distance	25–40 cm (30 cm)
Substrate temperature	300–500 °C (400 °C)

deposited for $0.2\,kg/cm^2$ air pressure is $10.153 \pm 0.001\,\text{Å}$, which is well above the reported value of bulk sample. Then, it reaches a minimum value of $10.107 \pm 0.001\,\text{Å}$ for the films deposited with $0.4\,kg/cm^2$, which is almost nearing the lattice constant of bulk sample $10.110\,\text{Å}$. Again, the lattice constant increases to $11.18 \pm 0.001\,\text{Å}$ for higher carrier gas pressures. The change in lattice constant for the deposited thin films over the bulk clearly suggests that the films have strains, which may be due to the change of lattice nature and concentration of the native imperfections. It is evident from the above characterization using XRD results that polycrystalline In_2O_3 films with $(2\,2\,2)$ preferred orientation can be prepared under the optimized process parameters given in Table 2 in parenthesis.

3.3. Surface morphological studies of In_2O_3 thin films

In_2O_3 thin films were prepared under the optimized deposition conditions at substrate temperatures 350, 400, and 450 °C and their surface morphologies were analyzed with the scanning electron micrographs and are shown in Fig. 5.

As seen from the figure, at low deposition temperatures, nonuniform surface and ill-defined grain formation is observed because of the amorphous nature of the films as revealed from the XRD results. The films deposited at 400, 450, and 500 °C were uniform, pinhole free and well covered and adherent to the glass substrate. However, the smoothest surface corresponds to highly crystalline In_2O_3 films grown at 400 °C, which is also having the highest XRD peak intensity and preferential orientation along $(2\,2\,2)$ direction. At high temperature, the number of nuclei is some what increased. This type of growth can be explained on the basis of differential nucleation for the chemical spray pyrolysed films and their dependence on substrate temperature. At lower temperatures, the solid melted and vaporized before droplets reached the substrate surface. Therefore, nuclei are formed on the substrate because of the gas-phase diffusion. Since the available activation energy for nucleation is less at lower temperature, number and size of nuclei are small leading to the formation of rough surface. At still higher temperature, thermal energy is sufficient for creating more number of
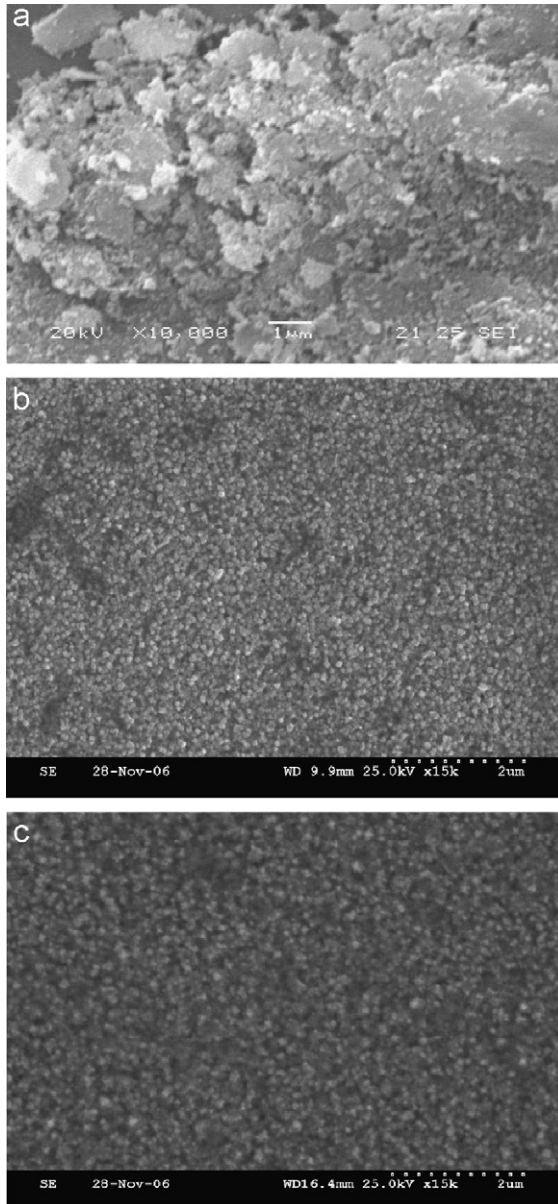
Carrier gas pressure decides the size of droplet which determines the heating rate and the residence time of the droplet during pyrolysis. For optimization, depositions were performed for different carrier gas pressures of 0.2, 0.3, 0.4, and $0.5\,kg/cm^2$ keeping the deposition temperature constant at 400 °C.

The XRD pattern of indium oxide films as a function of carrier gas pressure is shown in Fig. 4. It is clear that all the films are polycrystalline in nature and have $(2\,2\,2)$ preferred orientation. Another major orientation present is $(4\,0\,0)$, while other peaks like $(4\,4\,0)$ and $(6\,2\,2)$ are also seen with lower intensities. It can be observed that the films prepared using a pressure of $0.4\,kg/cm^2$ show a well-crystallized phase as evident from the sharp and intense peaks seen in Fig. 4c. Films prepared with 0.2 and $0.3\,kg/cm^2$ are less crystalline compared to that prepared with $0.4\,kg/cm^2$. For high flow rate ($0.5\,kg/cm^2$), the droplets formed were small and evaporation of solvent occurred which produced powdery particles on the substrate. This limits the In_2O_3 film growth, giving rise to a very thin film but with rough surface leading to less transmittance.

The variation of lattice constant with carrier gas pressure was calculated. The lattice constant of In_2O_3 films

Fig. 5. SEM images of In_2O_3 films prepared at substrate temperatures: (a) 350 °C, (b) 400 °C, and (c) 450 °C.

nuclei and in due course, they combine to form grains of bigger size due to lateral migration of nuclei. At the same time, films grown at higher substrate temperature above 400 °C show clusters and this type of growth is due to chemical reaction that takes place in the vapor phase. This limits the gas-phase diffusion on the substrate which might have caused a decrease in the grain growth at temperatures above the optimized substrate temperature.

The topography of In_2O_3 film surface deposited at 350, 400, and 450 °C was viewed three dimensionally (Fig. 6a–c) by atomic force microscopy (AFM). The AFM image of the film deposited at 350 °C (Fig. 6a) shows nonuniform surface with pits and patches. From the surface morphology of In_2O_3 film deposited at 400 °C (Fig. 6b), it is clearly observed that the film was uniformly covered over the glass

substrate without pinholes and the grain size distribution is uniform. Film deposited at 450 °C shows cluster formation as seen in Fig. 6c. These AFM surface topographies clearly show three-dimensional growth of In_2O_3 films prepared by the chemical spray pyrolysis technique [25].

The observed increase in grain size with substrate temperature can be explained on the basis of activation of atoms to move across the grown surface to the low-energy sites. As a result, the grain size of the films increases as a function of substrate temperature with subsequent influence upon the surface roughness. At higher deposition temperatures, i.e. above 400 °C, films are polycrystalline without any preferred orientations exhibiting clusters of smaller grains with larger surface roughness values. Grain sizes estimated from the AFM, SEM images, and XRD results are presented.

3.4. Compositional analysis by RBS

A tandem peletron accelerator is set up to deliver ions of 2 MeV He^+. The detector is shielded suitably so that it detects only the ions that have been backscattered at the backscattering angle 'θ'. The energy E_1 of the backscattered particle will be:

$$E_1 = E_0 K(M_2),$$

where $K(M_2)$ is the kinematic factor that depends only on the atomic mass of the target M_2. The backscattered signals are then amplified and fed to the multichannel analyzer. The RBS spectrum has been plotted between backscattered ions vs. energy for the prepared thin film samples. The peaks obtained correspond to different $K(M_2)$ values for backscattering from different elements present in the sample. Thus, from the position of the peaks in the backscattering spectrum, the elements present in the surface layer can be identified.

If the number of backscattered ions that make up the peaks is known, the elemental composition can be identified using the formula:

$$\frac{N_A}{N_B} = \frac{Y_A}{Y_B}\left(\frac{Z_B}{Z_A}\right)^2,$$

where N_A and N_B are the number of A and B atoms per unit area, Y_A and Y_B are the backscattering yield that make up the peaks of the elements A and B, respectively, and Z_A and Z_B are the respective atomic numbers of A and B.

A typical RBS of the In_2O_3 film deposited at 400 °C under the optimized spray conditions is shown in Fig. 7. The arrow indicates the position of the element at the surface of the film. The composition of the film calculated from the RBS data is found to be nearly stoichiometric but slightly oxygen deficient.

The elemental analysis was carried out only for the In and O elements. The atomic percentage of In/O was about 1.05 showing that the film is in good stoichiometry but with small oxygen deficiency.
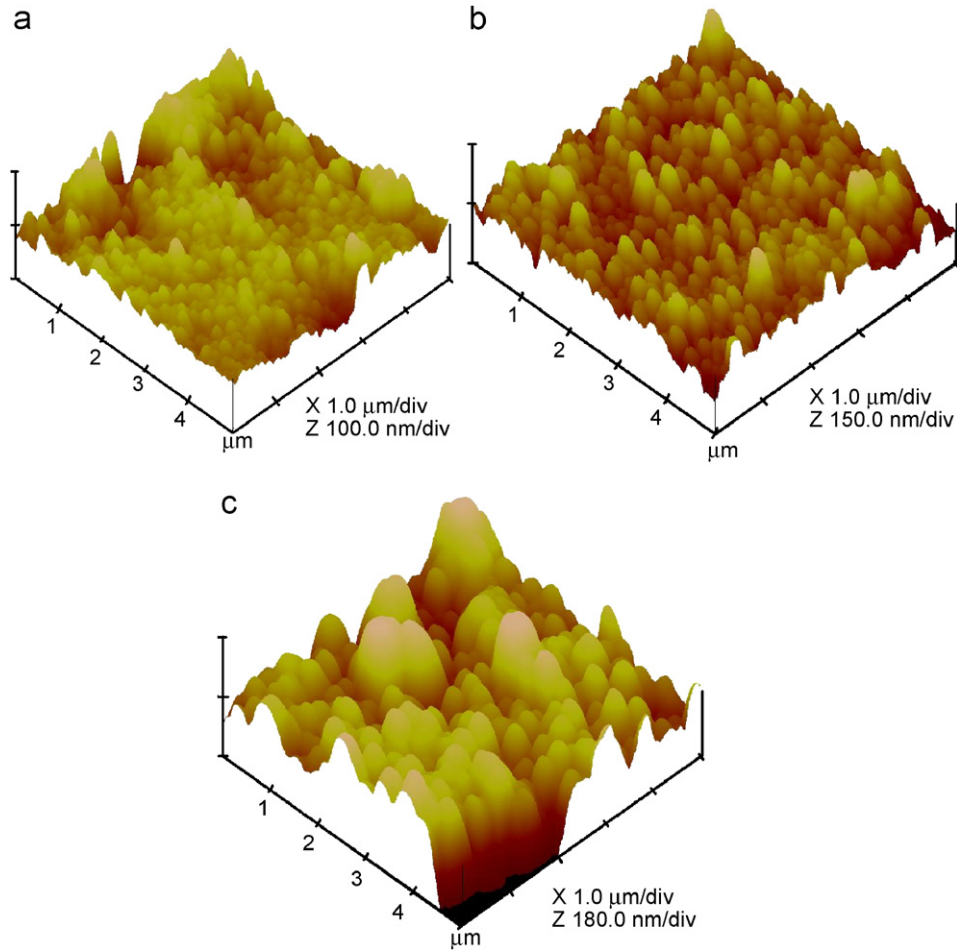
Fig. 6. AFM images of In$_2$O$_3$ films deposited at substrate temperatures: (a) 350 °C, (b) 400 °C, and (c) 450 °C.

3.5. Optical properties

In$_2$O$_3$ films prepared at various substrate temperatures between 300 and 500 °C under the optimized deposition conditions were subjected to optical characterization. The optical transmittance spectra of spray pyrolysed indium oxide films were recorded in the 300–1000 nm spectral region. From the measured spectral transmittance, the optical absorption coefficient (α), optical energy gap (E_g), refractive index (n), and extinction coefficient (k) are calculated using the method proposed by Swanepoel [26] using the transmittance spectrum in the transparent and weak/medium absorption region.

Fig. 8 shows the optical transmittance spectra of In$_2$O$_3$ films deposited at different substrate temperatures. The steep fall of transmittance for the films deposited at 400, 450, and 500 °C at the band edge confirms their well-crystallized nature. Films deposited at lower substrate temperatures, i.e. below 350 °C exhibited dark patches in the midst of foggy appearance and the transmittance is therefore less. The transmittance ($T\%$) in the visible region is found to increase with increasing substrate temperature. Maximum transmittance is observed for In$_2$O$_3$ films prepared at 400 °C. The increase in transmittance is
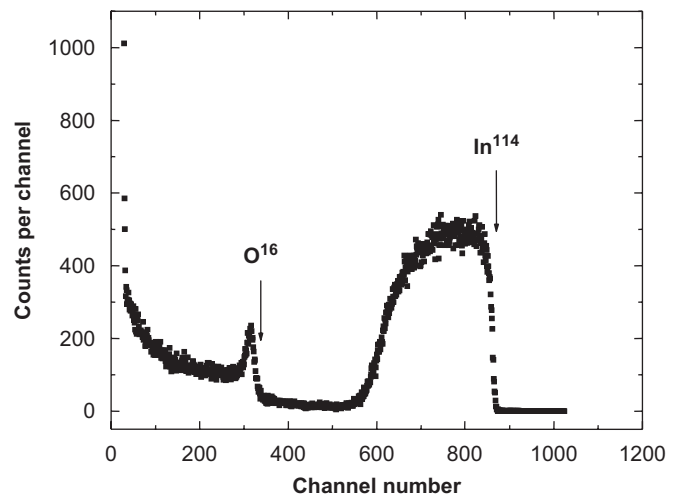

Fig. 7. RBS of In$_2$O$_3$ films deposited at 400 °C.

attributed to the uniform, well-adherent, and highly crystalline nature of the films as revealed from the XRD results that showed high peak intensities due to uniform oxidation and improvement in lattice arrangements [4]. In the case of higher substrate temperatures above 400 °C,
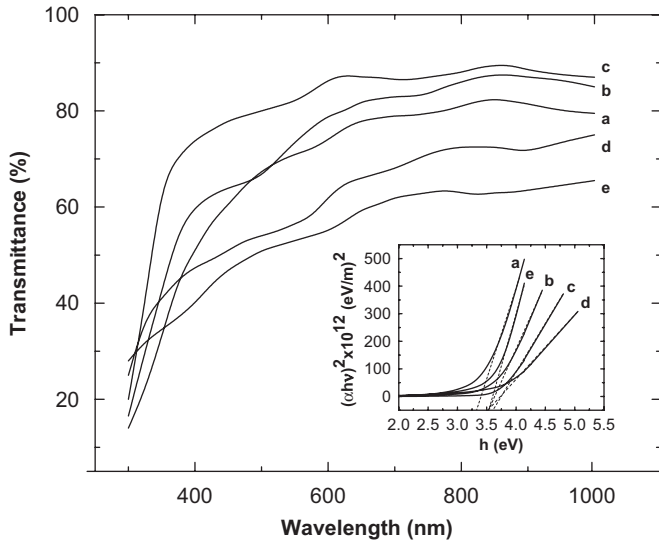
Fig. 8. Optical transmittance spectra of In$_2$O$_3$ films deposited at (a) 300 °C, (b) 350 °C, (c) 400 °C, (d) 450 °C, and (e) 500 °C and the inset shows $(\alpha h\upsilon)^2$ vs. $h\upsilon$ plot.

Fig. 9. Variation of refractive index and extinction coefficient with wavelength for In$_2$O$_3$ films deposited at 400 °C.

again there is a drop in the transmittance due to the impaired crystallinity as well as nonuniform and clustered surface morphology. Evaporation of solute at high deposition temperatures results in films with less stoichiometry. The impaired crystallinity produces less intense peak as evidenced from the XRD results.

Also, it is clearly observed that the transmittance spectra showed interference fringes due to the result of the interference of light reflected between the air/film and film/substrate interfaces. As the substrate temperature and the thickness of the film increase, the interference effects also become more prominent. The thickness of the sample measured from the interference maxima and minima values are almost nearer to the values obtained from the styles profiler.

From the measured spectral transmittance, the optical band gap values of polycrystalline In$_2$O$_3$ films are evaluated. The optical absorption α related to the optical band gap E_g of the prepared films at different substrate temperatures satisfies the equation:

$$\alpha h\upsilon = A(h\upsilon - E_g)^{1/2}. \tag{1}$$

The plots of $(\alpha h\upsilon)^2$ vs. $h\upsilon$ for the In$_2$O$_3$ films deposited at different temperatures is shown in the inset in Fig. 8. It can be seen that the plot is linear in the region of strong absorption, i.e. near the fundamental absorption edge. Extrapolation of the linear portion to $(\alpha h\upsilon)^2 = 0$ gives the direct allowed band gap values for the deposited films. The energy gaps of the films are found to vary from 3.53 to 3.68 eV. Such a shift in band gap to higher energies is attributed to the increased carrier density due to Brustein–Moss effect. This effect is due to the filling of states near the bottom of the lowest state in the conduction band [4]. This high value of band gap confirms the surface smoothness and uniformity of the In$_2$O$_3$ films prepared
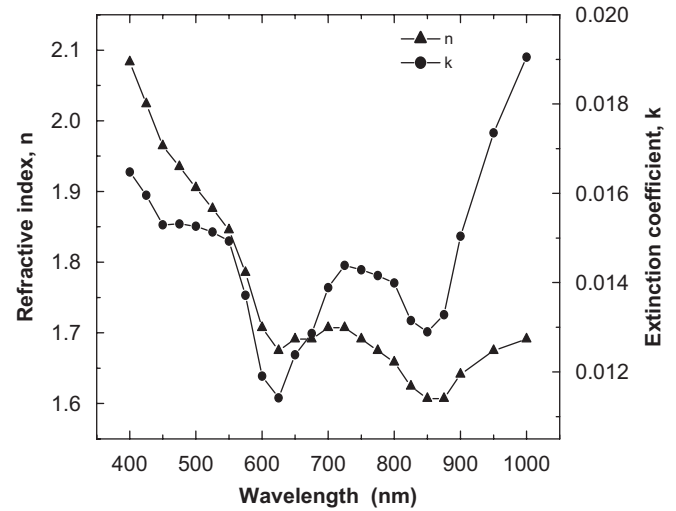
under the optimized spray conditions whose preferred orientation is along the (2 2 2) plane. This is in agreement with the observation that the band gap values of the order of 3.7–3.8 eV are associated with (2 2 2) orientation for the In$_2$O$_3$ films prepared by the reactive thermal evaporation technique [27].

The refractive index (n) and extinction coefficient (k) values are calculated for In$_2$O$_3$ film prepared at 400 °C for different wavelengths in the range 400–1000 nm. Fig. 9 shows the plot of refractive index and extinction coefficient as a function of wavelength λ for indium oxide film prepared at 400 °C.

The refractive index of the film decreases with the increase of λ and the rate of variation ceases at the higher wavelength region, i.e. $dn/d\lambda < 0$. This is consistent with what one would expect from Kramers Kroning analysis and the refractive index value at 500 nm is 1.905, which is very close to the reported value of 2.0 [28]. Further, the refractive index values are found to be lower for the films prepared at temperatures below and above 400 °C. The k values of indium oxide films are of the order of 10^{-2}, which is comparable to the reported values [29]. These values confirm the smoothness of the surface of the films deposited at the optimized spraying conditions. The increase in the value of k at longer wavelength region is due to interband absorption [30].

The dispersion relation for refractive index fits well and explains the variations obtained for indium oxide films. The dispersion energy E_d and the single oscillator energy E_o are obtained in terms of the single oscillator model and these values are related to the refractive index as

$$n^2 - 1 = \frac{E_d E_o}{E_o^2 - (h\upsilon)^2}. \tag{2}$$

The values of E_o and E_d for interband optical transitions are calculated and found to be 7.12 and 16.81 eV, respectively. From these values, the long wavelength limit

of refractive index n_α can be determined using the expression:

$$n_\alpha = \sqrt{1 + \frac{E_d}{E_o}}. \tag{3}$$

The long wavelength ($1/\lambda \approx 0$) limit refractive index of the In_2O_3 films prepared at 400 °C was calculated and the obtained value of $n_\alpha = 1.83$ is consistent with the reported values [17].

3.6. Dependence of electrical properties on process parameters

The variation of sheet resistance (R_{sh}) and electrical resistivity (ρ) of the In_2O_3 films, deposited at different temperatures, measured at room temperature (27 °C) and 127 °C is shown in Fig. 10a.

As seen, the sheet resistance and resistivity are found to decrease with increasing substrate temperature initially and then increase for films prepared at high deposition temperatures. For the films deposited at 400 °C, both the sheet resistance and resistivity are low. Further, it is evident

that on measuring sheet resistance and resistivity at elevated temperature 127 °C, the values are further decreasing compared to that measured at RT. The sheet resistance is found to decrease from 62 to 16 Ω with increase in deposition temperature from 300 to 400 °C. It is then increased to 25 Ω for high-temperature depositions. The sheet resistance measured at 125 °C for the film deposited at 400 °C exhibited the lowest sheet resistance value of 12 Ω.

The electrical resistivity was also found to decrease initially from the value of 2.25×10^{-3} Ω cm to 0.95×10^{-3} Ω cm for the films deposited in the temperature range 300–400 °C and then increase to 1.156×10^{-3} Ω cm for high-temperature (500 °C) deposited films. The same trend was observed when the measurements were done at 125 °C. In_2O_3 films deposited at 400 °C offered a low resistivity value of 0.69×10^{-3} Ω cm. Similar results on sheet resistance and resistivity variations with deposition temperatures were reported by Girtan and Folcher [18] and Byrant [31] for In_2O_3 thin films prepared by ultrasonic spray CVD process. The variations in the measured resistivity values with deposition temperature may be due to the film growth mechanism associated with the formation of nuclei and clusters. At the lower deposition temperatures, few nuclei are formed due to the availability of lower energy. The lower nucleation density is visible from the AFM surface images for the film deposited at 350 °C (Fig. 6a). However, many nuclei are formed by high-energy depositions and the grains are grown by the continuous diffusion of the gas phase leading to an increase in conductivity at 400 °C. At still higher deposition temperatures (>400 °C), the homogeneous reaction of the chemical species forms powdery surfaces that altered the conduction behavior of In_2O_3 films.

The hot probe measurement and the sign of the Hall coefficient have confirmed the n-type semiconducting nature of In_2O_3 films. The effect of deposition temperature on carrier concentration and Hall mobility are plotted in Fig. 10b.

It is observed that In_2O_3 films prepared here have high carrier concentration values of the order of 10^{20} cm^{-3} which reflects their degenerate character. Normally in In_2O_3 films, degeneracy arises even below this obtained value [32]. Fig. 10b shows that the carrier concentration increases up to the deposition temperature 400 °C and then shows a decreasing trend beyond 400 °C. This trend is attributed to the increased number of clusters and intergrain boundaries with increasing substrate temperature as seen from the SEM and AFM micrographs. These grain boundaries are the potential trap centers for charge carriers which reduce the carrier concentration. In the present study, it is evident from the XRD analysis that the crystallinity decreases at high deposition temperature due to lattice defects and this also supports the above-discussed electrical properties of In_2O_3 films.

The Hall mobility variation is also similar to that of carrier concentration, increases up to 400 °C and then
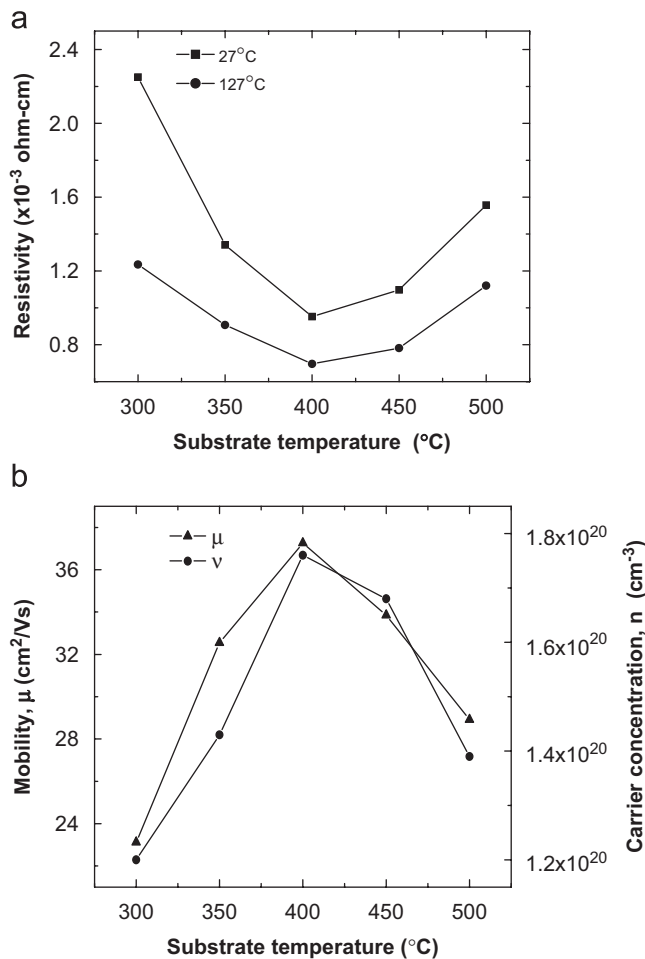
Fig. 10. Variation of (a) resistivity and (b) mobility and carrier concentration of In_2O_3 films deposited at different substrate temperatures.

decreases. A maximum value of 37.25 cm²/V s is obtained in the present study, and these values are consistent with the previously reported values [15]. The Hall mobility is influenced by the various scattering mechanisms, like grain boundary scattering, ionized impurity scattering, neutral impurity scattering, and scattering at other defects and dislocations [33]. In the present study, In₂O₃ films are predominantly (2 2 2) oriented due to which the number of scattering centers is minimum [34] and hence they have shown high mobility. To find whether reduction in grain boundary scattering is the main mechanism responsible for the increased mobility, the mean free path (l_n) values of carriers are calculated using the relation [33]:

$$l_n = \frac{h}{2e}\left[\frac{3n}{\pi}\right]^{1/3}\mu, \tag{4}$$

where n is the carrier (electron) concentration, μ is the Hall mobility, h is the Planck's constant, and e is the fundamental unit charge of electron.

The mean free path values of carriers calculated are in the range of 2.32–4.26 nm, which is very much smaller than the grain size values of 22–43 nm observed from XRD results and hence the grain boundary scattering is negligible. The carrier concentration value is varied between 1.2×10^{20} cm⁻³ and 1.7×10^{20} cm⁻³ and the mobility values show an increasing and decreasing trend with temperature which may be due to ionized impurity scattering [33].

The resistivity of In₂O₃ films prepared at different substrate temperatures was measured from room temperature to 150 °C and is shown in Fig. 11. For the region in which the electrical resistivity decreases with the increase of the temperature, all the In₂O₃ films satisfy the semiconductor resistivity dependent relation to temperature: $\rho = \rho_o(-E_a/kT)$, where $E_a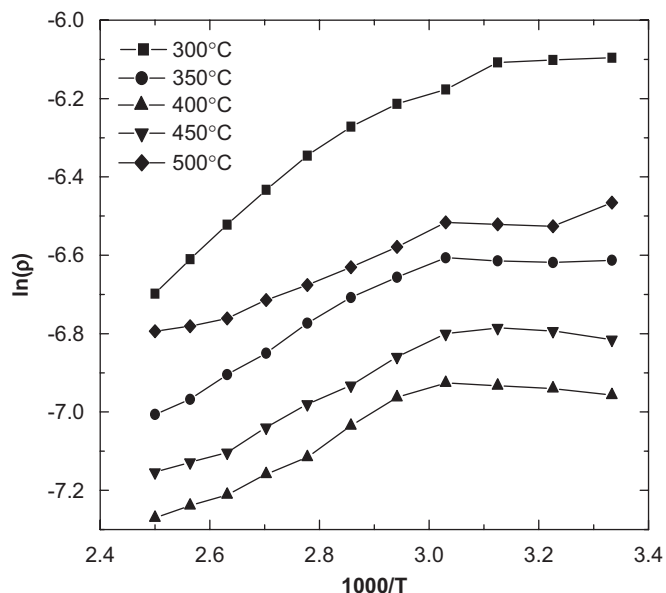$ denotes the thermal activation energy of electrical conduction, ρ_o represents a parameter related to the semiconducting nature of the material, and k is the Boltzmann's constant.

The calculated activation energy values of the indium oxide films deposited at substrate temperatures 300, 350, 400, 450, and 500 °C are 0.22, 0.17, 0.10, 0.12, and 0.90 eV, respectively. The activation energy decreases with the increase of substrate temperature. The values are of the same order of magnitude as the reported values [35].

In chemical spray pyrolysis deposition of thin films, the droplet size in the aerosol plays an important role in the reaction kinetics of the precursor, which again is reflected in the electrical conduction behavior. The droplet size also depends on the process parameter, SND which dictates the quality of the film that decides the conduction mechanism. The variation of resistivity (ρ), carrier concentration (n), and mobility (μ) with SND was studied by preparing In₂O₃ films by keeping SND at 25, 30, 35, and 40 cm. The resistivity values of the films prepared using these SND values are 0.018, 0.002, 0.014, and 0.020 Ω cm, respectively.

Fig. 12 shows the variation of carrier concentration and mobility as a function of SND. It is observed that both the values of n and μ reach a maximum for the SND of 30 cm and then decrease. These results show that the optimum value of SND for the preparation of good-quality In₂O₃ thin films is 30 cm for the present work. This dependence of electrical properties on SND can be understood by considering the forces acting on droplets inside the spray chamber.

The forces acting on the droplets when it travels from the nozzle towards the heated substrate surface are (i) the gravitational force that depends on the mass of the droplets, (ii) the frictional force between the droplet and air, and (iii) the force caused by temperature gradient in vapor phase (thermophoretic force). These forces would substantially change the reaction kinetics of the droplets. The thermophoretic force is the important force that acts on droplets before pyrolytic decomposition. The dependence of the thermophoretic force (F_{th}) on the radius of the
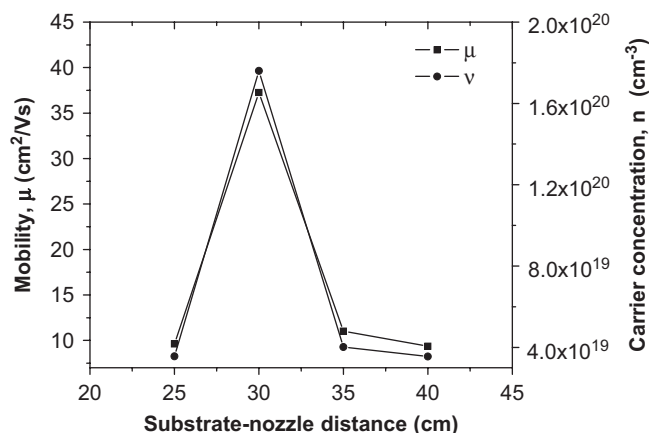

Fig. 11. Variation of ln(ρ) with measured temperature (T) for In₂O₃ films deposited at different substrate temperatures.

Fig. 12. Variation of carrier concentration and mobility with substrate–nozzle distance.

droplets is given by [16, 31]:

$$F_{th} = -\frac{3\pi\eta_a r_d}{\rho_a \lambda_a}, \tag{5}$$

where r_d is the radius of the droplets, T_d is the temperature, and λ_d is the thermal conductivity of the droplets. ρ_a is the density, η_a is the viscosity, λ_a is the thermal conductivity, and T_a is the temperature of air molecule.

Since the radius of the droplet 'r_d' is much larger than the mean free path of air molecules, then

$$\text{grad } T_d = \frac{3\lambda_a \text{ grad } T_a}{2\lambda_a + \lambda_d}, \tag{6}$$

where λ_d is the thermal conductivity of the droplets.

Assuming the distribution of the droplet sizes constant, the thermal energy gained by the droplets depends upon grad T_d factor. The thermal energy gained by the droplets will be greater with increasing SND. This leads to an enhanced pyrolytic reaction in the droplets as explained by Manifacier et al. [36]. SND = 30 cm seems to be the optimal distance as observed from the electrical properties. At this distance, the thermal energy gained by the droplet is sufficient to evaporate the solvent just above the surface leading to the heterogeneous reaction resulting in the formation of In_2O_3 films with optimum electrical properties and high conductivity.

For the indium oxide films prepared at distances below SND = 30 cm, the electrical values are found poor compared to the optimum values. At shorter SND, the thermal energy gained by the droplets is insufficient to vaporize the solvent completely. This residual solvent reduces the substrate temperature drastically and leads to homogeneous and incomplete reaction resulting films with white foggy surface. At high SND values greater than 30 cm, the heat energy gained by the droplets is high and the chemical reaction will be completed due to which the particle melts, vaporizes, and condenses as microcrystallites and powdery precipitate on the substrate surface. This homogeneous reaction limits the film growth resulting in reduced electrical and optical parameters.

4. Conclusion

The effect of deposition parameters on the structural, optical, and electrical properties of spray deposited indium oxide films has been studied elaborately. Variation of film thickness with substrate temperature and molarity of the precursor solution was studied. In_2O_3 films deposited at 400 °C with 0.008 M precursor exhibited a preferred orientation along the (2 2 2) direction and showed visible transmittance of 84%. The deposition temperature profoundly influenced the microstructures of In_2O_3 films as evident from the SEM and AFM morphologies. When the films were deposited at 400 °C with a substrate-to-nozzle distance of 30 cm, low resistivity, high carrier concentration and mobility values were obtained. It has been established that spray pyrolysis of a water–ethanol solution of In-acac at 400 °C is a simple route for deposition of transparent and conducting indium oxide films on glass substrates which can be used as either conducting or transparent electrodes in optoelectronic devices.

References

[1] O.N. Mryasor, A.J. Freeman, Phys. Rev. B64 (2001) 233111.
[2] R.G. Gordon, Mater. Res. Soc. Bull. 25 (2000) 52.
[3] H. Mexiner, J. Gerblinger, U. Lampe, M. Fleisher, Sens. Actuators B B23 (1995) 119.
[4] K.L. Chopra, S.R. Das, Thin Film Solar Cells, Plenum Press, New York, 1983.
[5] K.G. Gopachandran, B. Joseph, J.T. Abraham, P. Koshy, V.K. Vaidyan, Vacuum 86 (1997) 547.
[6] C.G. Granquist, Sol. Energy Mater. Sol. Cells 60 (2000) 2301.
[7] B.-S. Chious, J.-H. Tsai, J. Mater. Sci.: Mater. Electron. 10 (1999) 491.
[8] G. Parthasarathy, C. Adachi, P.E. Burrows, S.R. Forrest, Appl. Phys. Lett. 76 (2000) 2128.
[9] J. Tamaki, C. Naruo, Y. Yamamoto, M. Matusuoka, Sens. Actuators B 83 (2002) 190.
[10] J.Q. Hu, F.R. Zhu, J. Zhang, H. Gong, Sens. Actuators B 93 (2003) 175.
[11] V. Marotta, S. Orlando, G.P. Parisi, A. Giardini, G. Perna, A.M. Santoro, V. Capozzi, Appl. Surf. Sci. 168 (2000) 141.
[12] J.K. Sheu, Y.K. Su, G.C. Chi, M.J. Jou, C.M. Chang, Appl. Phys. Lett. 72 (1999) 3317.
[13] T. Maruyama, K. Fukui, J. Appl. Phys. 70 (1991) 3848.
[14] A. Gurlo, M. Ivanovskaya, A. Pfau, U. Weimar, W. Gopel, Thin Solid Films 307 (1997) 288.
[15] J. Joseph Prince, S. Ramamurthy, B. Subramanian, C. Sanjeeviraja, M. Jayachandran, J. Cryst. Growth 240 (2002) 142.
[16] W. Siefert, Thin Solid Films 121 (1984) 275.
[17] P.K. Manoj, K.G. Gopachandran, P. Koshy, V.K. Vaidyan, B. Joseph, Opt. Mater. 28 (2006) 1405.
[18] M. Girtan, G. Folcher, Surf. Coat. Technol. 172 (2003) 242.
[19] C.H. Lee, C.S. Huang, Mater. Sci. Eng. B22 (1994) 233.
[20] A. Ayouchi, M. Martin, D. Leinen, J.R. Ramos-Barrado, J. Cryst. Growth 247 (2003) 497.
[21] W. DeSisto, M. Sosnowski, F. Smith, J. Deluca, R. Kershan, K. Dwight, A. World, Mater. Res. Bull. 24 (1989) 753.
[22] A. El Hichou, A. Kachonane, J.L. Bubenorff, M. Addou, J. Ebothe, M. Troyon, A. Bougrine, Thin Solid Films 458 (2004) 263.
[23] A. Ashor, N. El-Kadry, M.R. Ebid, M. Farghal, A.A. Ramadan, Thin Solid Films 279 (1996) 242.
[24] C. Agashe, D.J. Goyal, B.R. Marathe, M.G. Takwala, V.G. Bhide, Mater. Lett. 11 (1991) 363.
[25] G. Koretcenkov, V. Brinzari, M. Ivanov, A. Cerneavschi, J. Rodriquez, A. Cirera, A. Cornet, J. Morante, Thin Solid Films 479 (2005) 38.
[26] R. Swanepoel, J. Phys. E: Sci. Instrum. 16 (1983) 1214.
[27] P. Thilakan, J. Kumar, Vacuum 48 (1997) 463.
[28] D.S.D. Amma, V.K. Vaidyan, P.K. Manoj, Mater. Chem. Phys. 93 (2005) 194.
[29] K.S. Ramaih, V.S. Raja, A.K. Bhatnagar, R.D. Tomlinson, R.D. Pikington, A.E. Hills, S.J. Chang, Y.K. Su, F.S. Juang, Semicond. Sci. Technol. 15 (2000) 676.
[30] M. Girtan, Mater. Sci. Eng. B118 (2005) 175.
[31] W.A. Byrant, J. Mater. Sci. 12 (1977) 1285.
[32] V. Vasu, A. Subramanyam, Thin Solid Films 193–194 (1990) 696.
[33] G. Sanson, R. Rup, A. Mansingh, Thin Solid Films 190 (1990) 287.
[34] M.G. Takawala Chitra Agashe, V.G. Bhide, J. Appl. Phys. 70 (1991) 7382.
[35] A.S. Ryzhikov, R.B. Vasiliev, M.N. Ruyantseva, Mater. Sci. Eng. B96 (2002) 268.
[36] J.C. Manifacier, L. Szepessay, J.F. Bresse, M. Perotin, R. Stuck, Mater. Res. Bull. 14 (1979) 163.